Imaging cellular signals in the heart *in vivo*: Cardiac expression of the high-signal Ca^{2+} indicator GCaMP2

Yvonne N. Tallini*†, Masamichi Ohkura†‡, Bum-Rak Choi†§, Guangju Ji*, Keiji Imoto¶, Robert Doran*, Jane Lee*, Patricia Plan§, Jason Wilson*, Hong-Bo Xin*, Atsushi Sanbe‖, James Gulick‖, John Mathai**, Jeffrey Robbins‖, Guy Salama§, Junichi Nakai††, and Michael I. Kotlikoff*‡‡

*Biomedical Sciences, College of Veterinary Medicine, Cornell University, Ithaca, NY 14850; ‡First Department of Pharmacology, School of Pharmaceutical Sciences, Kyushu University of Health and Welfare, Yoshino, Nobeoka 882-8508, Japan; Departments of §Cell Biology and Physiology and **Medicine, University of Pittsburgh School of Medicine, Room S 314 Biomedical Science Tower, 200 Lothrop Street, Pittsburgh, PA 15261; ¶Department of Information Physiology, National Institute for Physiological Sciences, Myodaiji, Okazaki 444-8585, Japan; ‖Division of Molecular Cardiovascular Biology, Cincinnati Children's Hospital, 3333 Burnet Avenue, Cincinnati, OH 45229; and ††Laboratory for Memory and Learning, RIKEN Brain Science Institute, 2-1 Hirosawa, Wako-shi, Saitama 351-0198, Japan

Edited by Richard L. Huganir, Johns Hopkins University School of Medicine, Baltimore, MD, and approved January 26, 2006 (received for review October 27, 2005)

Genetically encoded sensor proteins provide unique opportunities to advance the understanding of complex cellular interactions in physiologically relevant contexts; however, previously described sensors have proved to be of limited use to report cell signaling *in vivo* in mammals. Here, we describe an improved Ca^{2+} sensor, GCaMP2, its inducible expression in the mouse heart, and its use to examine signaling in heart cells *in vivo*. The high brightness and stability of GCaMP2 enable the measurement of myocyte Ca^{2+} transients in all regions of the beating mouse heart and prolonged pacing and mapping studies in isolated, perfused hearts. Transgene expression is efficiently temporally regulated in cardiomyocyte GCaMP2 mice, allowing recording of *in vivo* signals 4 weeks after transgene induction. High-resolution imaging of Ca^{2+} waves in GCaMP2-expressing embryos revealed key aspects of electrical conduction in the preseptated heart. At embryonic day (e.d.) 10.5, atrial and ventricular conduction occur rapidly, consistent with the early formation of specialized conduction pathways. However, conduction is markedly slowed through the atrioventricular canal in the e.d. 10.5 heart, forming the basis for an effective atrioventricular delay before development of the AV node, as rapid ventricular activation occurs after activation of the distal AV canal tissue. Consistent with the elimination of the inner AV canal muscle layer at e.d. 13.5, atrioventricular conduction through the canal was abolished at this stage. These studies demonstrate that GCaMP2 will have broad utility in the dissection of numerous complex cellular interactions in mammals, *in vivo*.

atrioventricular node | Ca^{2+} imaging | genetic sensor | heart development | fluorescent Ca^{2+} sensor

Transient, highly regulated elevations in cytosolic free Ca^{2+} underlie numerous cellular processes that enable organ function (1–5). In the mammalian heart, for example, efficient function depends upon the coordinated release and reuptake of Ca^{2+} ions from intracellular organelles in millions of cells, at rates between 0.5 and 15 Hz throughout life, and even subtle dysfunctions of this process can result in cardiac arrythmias and sudden death. Whereas fluorescent imaging using purpose-designed small Ca^{2+}-binding indicator molecules has enabled important advances in the understanding of the regulatory processes underlying Ca^{2+} signaling in single cells (6, 7), these approaches have significant limitations in the context of a complex, multicellular organ such as the beating heart. Thus, difficulties in obtaining an adequate and stable concentration of indicator molecules within cells deep in complex tissues, the incompatibility of loading procedures in the *in vivo* setting, and the inability to selectively load specific cell lineages constitute substantial experimental constraints on the study of multicellular, processive Ca^{2+} signaling in complex organ function. Genetically encoded sensors of Ca^{2+} signaling (7–13) hold great promise in this regard and have been used to study signaling in lower organisms (14–17), but they have not been effectively used in mammals *in vivo* because of poor intrinsic signal strength, alinearity, inadequate temperature stability, or perturbing interactions between the sensing molecule and endogenous cellular proteins (18–21). Recently Pologruto *et al*. (21) illustrated this point by a careful comparison of the performance of GCaMP1 (11), Camgaroo2 (22), and Inverse Pericam (12) with the small molecule Ca^{2+} probes X-Rhod-5F and Fluo4-FF in brain slices, demonstrating the inability of the genetic indicators to detect physiologic, low-frequency action potential Ca^{2+} transients (see also ref. 23). Here, we report a markedly improved genetically encoded Ca^{2+} reporter molecule based on circular permutation of GFP (cpGFP) (10–12), its conditional expression in the hearts of transgenic mice, and the use of the sensor to monitor Ca^{2+} transients in the beating heart of adult and embryonic mice *in vivo* and *in vitro*.

Results and Discussion

Development of GCaMP2. Designed and random alterations in the previously described, circularly permutated eGFP-based, Ca^{2+}-sensing molecule, which we now term GCaMP1 (11), were undertaken to improve brightness and stability. Ca^{2+}-dependent fluorescence of GCaMP arises from the interaction between Ca^{2+}/calmodulin at the C terminus of cpGFP and an N-terminal myosin light chain kinase (MLCK) fragment. GCaMP1 has only a fraction of the brightness of the parent eGFP molecule and is unstable at physiological temperatures. To address these deficiencies, three mutations were first introduced into GCaMP1: V163A, S175G, and A206K (Fig. 1*a*); V163A and S175G are previously described mutations that improved the temperature stability of GFP (24), whereas the A206K was introduced to prevent GFP dimerization (25). V163A and S175G mutations in GCaMP1 were previously reported as GCaMP1.6 (26), result in an intermediate improvement in the brightness of GCaMP1, but neither these mutations or A206K correct the instability above 30°C. A plasmid leader sequence (RSET) was attached to the N terminus for purification, GCaMP1.6 cDNA was subjected to PCR-based random mutagenesis, and bacterial colonies displaying the brightest fluorescence at 37°C were picked and sequenced (see *Materials and Methods*). This

Conflict of interest statement: No conflicts declared.

This paper was submitted directly (Track II) to the PNAS office.

Abbreviations: αMHC, α myosin heavy chain; cpGFP, circularly permutated GFP; AV, atrioventricular; e.d., embryonic day; tTA, tetracycline transactivator allele; iso, isoproterenol; dox, doxycycline; ccGC2, ccGCaMP2^{+}/tTA^{+}.

Data deposition: The sequence reported in this paper has been deposited in the GenBank database (accession no. DQ381402).

†Y.N.T., M.O., and B.-R.C. contributed equally to this work.

‡‡To whom correspondence should be addressed. E-mail: mik7@cornell.edu.

PHYSIOLOGY

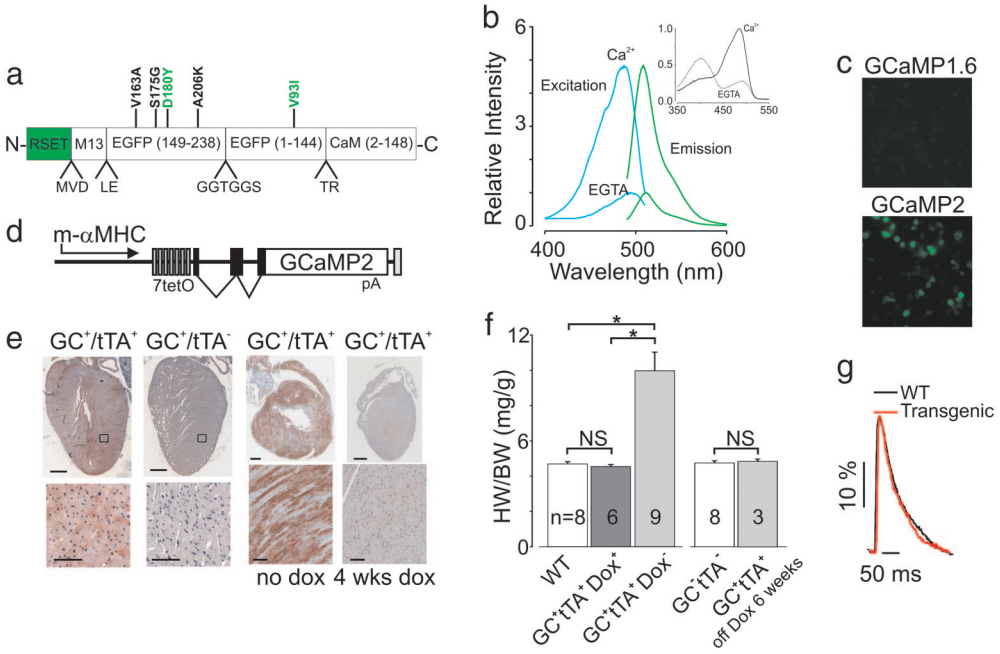

Fig. 1. Conditional cardiac GCaMP2 mice (ccGC2). (*a*) GCaMP2 consists of circularly permutated eGFP with the molecule interrupted at residue 145 and a 13-residue peptide of myosin light chain kinase (M13) and calmodulin (CaM), placed at the new N and C termini, respectively. An RSET polyHis peptide was introduced N-terminal to the original methionine reported as part of GCaMP1 (11). Mutations resulting in augmented brightness and thermal stability are shown in green. (*b*) Excitation and emission spectra for GCaMP2 in chelating (10 mM EGTA) and saturating (10 mM) Ca^{2+} solutions. At saturating Ca^{2+}, the spectral characteristics are similar to eGFP (Table 1). (*Inset*) Absorption spectra. (*c*) Comparison of brightness/thermal stability of GCaMP1.6 and GCaMP2 in transiently transfected HEK cells cultured at 37°C for 1 day indicates retention of brightness in GCaMP2. Images were obtained in unstimulated cells at ×20 magnification by using the same exposure time and camera gain. (*d*) Transgene design including the weakened αMHC promoter, tet operator sequences (tetO), noncoding exons, kozak sequence, GCaMP2 cDNA sequence, and polyA recognition sequence. (*e*) Control of transgene expression by tTA (left two images) and silencing of transgene after 4 weeks of doxycycline (dox) administration (right two images). GCaMP2 was detected by anti-GFP staining (38); areas of sections (*Lower*) are indicated by boxes. [Scale bars: 1 mm (*Upper*) and 100 μm (*Lower*).] (*f*) Heart weight/body weight (HW/BW) ratios of age-, sex-, and litter-matched mice. Hearts from ccGC2 transgenic mice maintained on dox from birth were not significantly (NS) different from control (one-way ANOVA), whereas double transgenic mice not maintained on dox had significant heart enlargement (*, $P < 0.05$). Cardiomegaly was prevented by maintenance of mice on dox, followed by removal at 13–15 weeks. (*g*) Optical Ca^{2+} transients recorded in isolated/perfused WT and ccGC2 hearts indicate that the Ca^{2+} transient is not altered by expression of the transgene. Hearts were transiently loaded with Rhod2 and paced at 350/min, and an equivalent ventricular region was recorded by using a photodiode array (40).

process identified two new mutations (D180Y and V93I) in separate β-sheets that improved the brightness of the cpGFP molecule. The addition of the N-terminal 35-residue polyHis RSET linked to the MLCK sequence was critical for thermal stability, because removal of the leader sequence led to loss of fluorescence at 37°C. The RSET-M13-cpGFP-calmodulin molecule GCaMP2 (GenBank accession no. DQ381402) is, respectively, ≈200 times and 6 times brighter than GCaMP1 and GCaMP1.6, and displays a similar 4- to 5-fold increase in signal between 0 and saturating Ca^{2+} (Fig. 1*b*; Table 1). Most importantly, the thermal stability of GCaMP2 results in retained high brightness at 37°C (Fig. 1*c*). Titrations of purified GCaMP2 protein with fixed Ca^{2+} solutions indicated highly cooperative Ca^{2+} binding over the physiological range of cellular free Ca^{2+} (K_D = 146 nM; Hill coefficient = 3.8), with no significant Mg^{2+} dependence (data not shown). The high brightness, thermal stability, and large dynamic range of GCaMP2 constitute significant attributes relative to previously reported genetic Ca^{2+} sensors (refs. 11, 12, and 22 and Table 1), suggesting that the molecule may enable the detection of physiological Ca^{2+} signals in mice *in vivo*. A previous report (27) has described the use of GCaMP2 for *in vitro* measurements.

Table 1. Spectral characteristics of GCaMPs

Name	Ca^{2+}	λ_{abs} (ε)	λ_{em} (Φ)	Brightness ($\varepsilon \times \Phi$)
G-CaMP1	−	409 (1,100)		
		488 (570)	510 (0.03)	17
	+	410 (690)		
		487 (1,400)	510 (0.05)	70
G-CaMP1.6	−	404 (5,800)		
		489 (1,100)	510 (0.56)	616
	+	403 (5,200)		
		488 (3,800)	509 (0.79)	3,002
G-CaMP2	−	400 (11,100)		
		491 (5,200)	511 (0.70)	3,640
	+	401 (5,800)		
		487 (19,000)	508 (0.93)	17,670

Transgenic Mice Conditionally Expressing GCaMP2 in Heart Cells. We conditionally expressed GCaMP2 in heart cells using a tet-Off system, to avoid potential pathology associated with high expression of a Ca^{2+}-binding protein in myocytes. GCaMP2 was placed downstream of a weakened α myosin heavy chain (ΔαMHC) promoter and seven tetO enhancer sequences (28) (Fig. 1*d*). Six founder lines (ccGCaMP2 mice) were crossed with hemizygous αMHC-tetracycline transactivator allele (tTA) transgenic mice expressing the hybrid transactivator protein (28) and screened for transgene expression in the absence of doxycycline (dox). Three lines of ccGCaMP2 were selected as having strong, homogenous transgene expression in all areas of the heart and minimal or no leak expression of GCaMP2 in the absence of the tetracycline transactivator allele (tTA-mice) (Fig. 1*e*). As expected, transgene expression in the hearts of double transgenic [ccGCaMP2$^+$/tTA$^+$ (ccGC2)] mice was restricted to myocytes, with no staining observed in endocardial, coronary vascular smooth muscle, or nonmuscle tissues; expression was observed in smooth muscle in the large pulmonary arteries, likely reflecting the derivation of these tissues from myocardium (29). Administration of dox for 2–5 weeks resulted in a time-dependent decrease of transgene expression, with almost complete suppression by 3–4 weeks (Fig. 1*e*). Unregulated expression of GCaMP2 from birth resulted in significant cardiomegaly in adult double transgenic mice, similar to that reported in mice with targeted overexpression of calmodulin (30). However, heart size in mice maintained on dox from birth and hearts from GCaMP2$^+$ or tTA$^+$ single transgenic mice were not enlarged

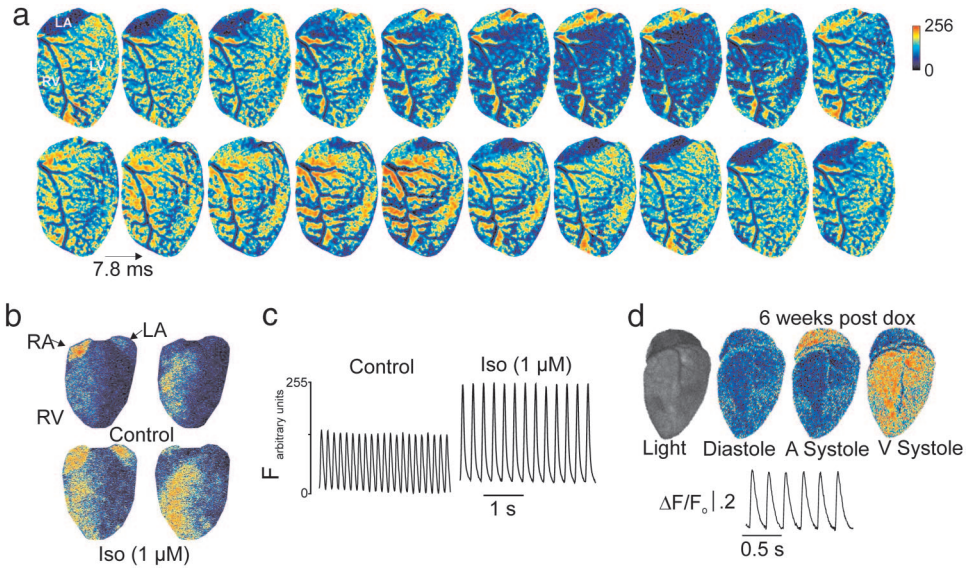

Fig. 2. *In vivo* Ca^{2+} signaling. (*a*) Sequential images of Ca^{2+}–dependent fluorescence during a single cardiac cycle in an anesthetized and ventilated mouse. Images were obtained at 128 Hz with an Andor iXon camera. Note lack of fluorescence in cardiac vasculature and decline of ventricular Ca^{2+} transient during beginning of atrial systole (very top of image) (full sequence available in Movie 1). (*b*) Ca^{2+} fluorescence in a 1-day-old mouse *in vivo*. Images at peak atrial and ventricular systole are shown from a series obtained at 33 Hz. Sequences show before (*Upper*) and directly after (*Lower*) direct application of 10 μM isoproterenol (Iso). The heart is illuminated obliquely from the left side of the camera, highlighting right atrium (RA) and ventricle (RV); each series was separately scaled from 0 to 255 (LA, left atrium). See also Movie 3. (*c Left*) Ca^{2+} transients recorded from the atrium (3 × 3 pixels) in experiment shown in *b*; (*Right*) transients recorded from same heart after direct application of 10 μM iso. (*d*) *In vivo* images from a phenotypically normal heart after transgene induction by dox removal. Images show diastole and peak atrial (A) and ventricular (V) systole. Continuous ventricular fluorescence from full experiment is shown below. Color scale in *a* applies throughout.

relative to strain-matched WT controls (Fig. 1*g*), further demonstrating effective regulation of transgene expression by dox. Because GCaMP2 expression is effectively regulated, ccGC2 mice should be useful for the study of cardiac hypertrophy during controlled induction. To demonstrate that this phenotype can be effectively avoided, mice were maintained on dox starting *in utero* until 13–15 weeks and then removed for up to 6 weeks, and transgene expression was monitored. No cardiomegaly was detected up to 6 weeks after withdrawal (Fig. 1*f*), whereas transgene expression was detected by 2 weeks and robust functional signals were recorded beginning 4 weeks after withdrawal (see below). We confirmed that expression of GCaMP2 does not itself alter excitation–contraction coupling characteristics of heart cells by transiently loading control and transgenic hearts with the Ca^{2+}-sensitive dye Rhod2. In four transgenic and age-matched control hearts, the amplitude and duration of Rhod2 ventricular Ca^{2+} transients were not significantly different (Fig. 1*g*).

Optical Measurements of Ca^{2+} Transients in the Heart *in Vivo*. A prominent increase in eGFP fluorescence was observed *in vivo* in open-chested, ventilated, ccGC2 mice in all heart regions with every systole. As shown in Fig. 2*a* and Movie 1, which is published as supporting information on the PNAS web site, Ca^{2+}-dependent fluorescence was restricted to cardiac muscle, resulting in the highlighting of the vasculature pattern by the surrounding fluorescent cardiac myocytes. The increase in fluorescence observed between end diastole and peak systole varied between ≈0.5 and 1.5 ($\Delta F/F_{diastole}$) in spontaneously beating, adult hearts, and high signal/noise Ca^{2+} transients could be measured in all areas of the surface without constraining heart motion. Similar results were obtained in neonatal mice as early as 1 day after birth (Fig. 2*b*), although the level of transgene expression was more modest at this stage. Inotropic stimulation of the heart with isoproterenol (iso) resulted in a marked augmentation in end-diastolic and peak-systolic GCaMP2 fluorescence, and in the amplitude and rate of rise of the Ca^{2+}-dependent fluorescent transients, which were obtained from individual heart regions as small as 30 μm^2 beginning at postnatal day 1 (Fig. 2 *b* and *c*). *In vivo* recordings were also obtained from phenotypically normal mice withdrawn from dox for 4–6 weeks (Fig. 2*d*), indicating the ability to experimentally circumvent cardiac hypertrophy. To our knowledge, there are no previously reported measurements of cellular Ca^{2+} transients in the mammalian heart *in vivo*, or while the heart is pumping against a physiological load.

Optical Measurements of Ca^{2+} Transients in the Isolated, Perfused Heart. To more quantitatively examine GCaMP2 signaling in the intact heart, cellular Ca^{2+} transients from the heart surface were recorded in spontaneously beating, isolated, perfused hearts by using photodiode arrays or a high-speed complementary metal oxide semiconductor (CMOS) camera (see *Materials and Methods*). The high brightness of GCaMP2 enabled the recording of Ca^{2+}

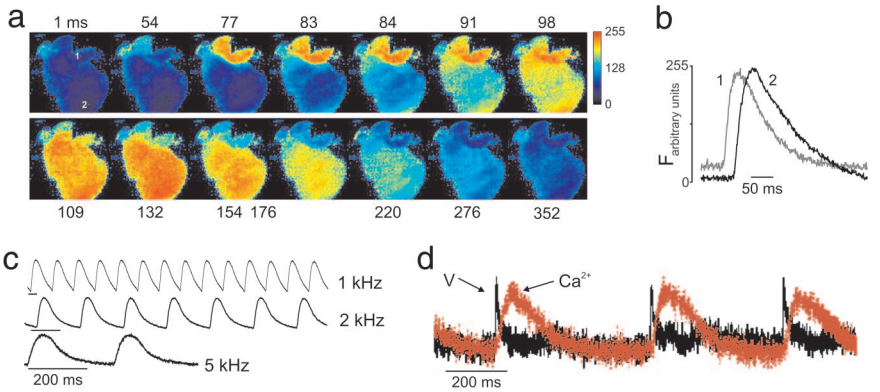

Fig. 3. *In vitro* Ca^{2+} signaling. (*a*) Single spontaneous contraction in an isolated, perfused adult heart recorded at 1 kHz with a Micam Ultima 100 × 100 pixel CMOS camera. Images are selected to show major phases of the conduction of the atrial and ventricular Ca^{2+} wave (full sequence available in Movie 3). (*b*) Fluorescence from a single pixel in atrium and ventricle from series shown in *a* (area indicated in first frame; ≈40 × 40-μm area). (*c*) Typical transients recorded with a CMOS camera showing signal/noise characteristics of ventricular Ca^{2+} transients at different pacing rates. Transients are unprocessed fluorescence values from a single pixel recorded at the frame rates indicated at right, normalized for comparison. (*d*) Simultaneous recording of action potential (RH237) and GCaMP2 Ca^{2+} transient from same ventricular (V) region with a photodiode array.

PHYSIOLOGY

signals with excellent signal/noise characteristics and spatial resolution over the entire heart surface (Fig. 3*a* and Movie 2, which is published as supporting information on the PNAS web site). Fluorescent transients in paced hearts were not altered by inhibition of contraction with 2 μM cytochalasin D, indicating a lack of significant motion artifact in this system (data not shown). Transients recorded at frame rates as high as 5 kHz from a single pixel comprising a spatial dimension of $\approx$40 μm^2, or <10 myocytes, were highly stable, providing reproducible Ca^{2+} signals from all heart regions for up to 5 h without signal/noise deterioration or loss of signal amplitude (Fig. 3 *b* and *c*). In a series of experiments, the conduction velocity of the Ca^{2+} transient was 24.1 $\pm$ 3.7 cm/s and increased 8–20% after perfusion with 1 μM iso. The spectral separation between GCaMP2 and commonly used potentiometric dyes (31) also allowed the simultaneous optical recordings of action potential and Ca^{2+} transients using spatially registered photodiode arrays (32). GCaMP2-expressing hearts were briefly loaded with RH237, illuminated at wavelengths that excited both indicators, and imaged with spatially registered photodiode arrays (Fig. 3*d*). Action potentials and Ca^{2+} signals were recorded from the same heart regions in spontaneously beating and paced hearts; the presence of the Ca^{2+} indicator in cardiac cytosol did not alter the characteristics of cardiac action potentials.

Biophysical Characteristics of GCaMP2 *in Vivo*. When expressed as transgenes in animals, genetically encoded sensors undergo unpredictable changes in photochemical properties, most likely because of interactions between the indicator and endogenous proteins, resulting in a marked degradation of indicator signaling properties relative to those observed in transiently transfected cells in tissue culture (20, 21, 23). To determine the behavior of GCaMP2 in this context, we compared Ca^{2+}-dependent fluorescence of heart cytosol from ccGC2 mice with GCaMP2 protein purified from bacteria. The Ca^{2+} affinity of GCaMP2 in cardiac cytosol was somewhat lower than the purified protein (K_D 188 versus 146 nM), but the Hill slope (3.8) was equivalent and the high indicator dynamic range was maintained (data not shown). An equivalent shift was detected by using cardiomyocytes isolated from transgenic hearts and fixed Ca^{2+} concentrations in the presence of ionomycin (data not shown). We estimated the concentration of GCaMP2 expressed in ccGC2 mouse hearts at 1.6 μM, by comparing the magnitude of fluorescence of diluted cytosol (488/508) under saturating Ca^{2+} conditions with that of the purified protein.

Fusion protein indicators such as GCaMP2 undergo complex transitions to and from the photoactive state, potentially resulting in kinetic discrepancies between the underlying signal and emitted fluorescence. In the context of rapid Ca^{2+} signaling in the heart, these transition delays would be expected to result in a significant distortion of the underlying rapid Ca^{2+} transient kinetics and might be affected by interaction with endogenous proteins. We examined the fluorescence association and dissociation kinetics of GCaMP2 in ccGC2 heart cytosol in stop-flow experiments and compared these with the purified protein. As shown in Fig. 4 *a* and *b* and Table 2, the association time constant was $\approx$14 ms and did not vary significantly as a function of cytosol concentration; addition of purified GCaMP2 protein to cardiac cytosol also did not alter the association kinetics (data not shown). The fluorescence association rate constant of the purified protein was equivalent to that of cardiac cytosol, indicating that neither competing Ca^{2+} buffers within the cytosol nor interactions between GCaMP2 and cytosolic proteins significantly alter the kinetic performance of GCaMP2. The dissociation time constant was $\approx$75 ms for cardiac cytosol, which was equivalent to purified protein and unaffected by cytosol dilution or addition of recombinant GCaMP2 (Table 2). Thus, the association and dissociation time constants for GCaMP2 are markedly faster than reported for GCaMP1 (11), almost certainly because of evaluation of the less stable GCaMP1 kinetics at room temperature; not surprisingly decreases in temperature similarly

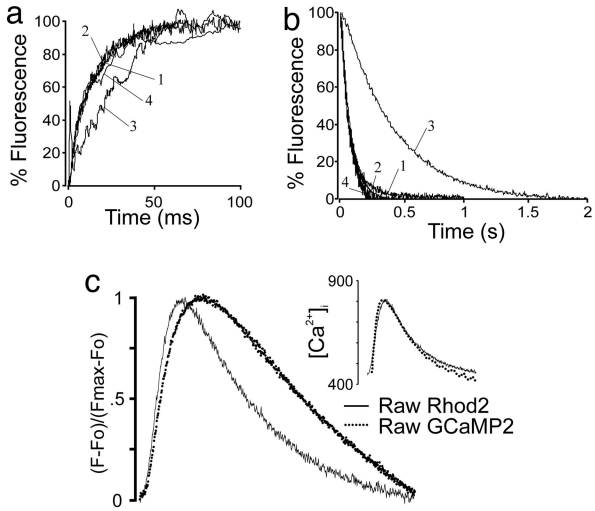

Fig. 4. Kinetics of GCaMP2. (*a*) Fluorescence association kinetics in stop-flow experiment. Traces 1–3 are dilutions of GCaMP2 cardiac cytosol and protein in solution. Trace 4 is cardiac cytosol recorded at 20°C. Values for exponential fits and full conditions are in Table 1. Note equivalence of association time course despite different Ca^{2+} jump levels and/or purified protein or cardiac cytosol (traces 1, 2, and 4). (*b*) Dissociation kinetics in same conditions as *a*. Note markedly slowed off-rate at 20°C (trace 3). (*c*) Simultaneous recordings of Rhod2 and GCaMP2 Ca^{2+} fluorescence. Average raw fluorescence values from five sequential cycles obtained from the same $\approx$30-μm^2 region of ventrical are shown (pacing rate = 300 per min). Note more rapid rise time and decay of Rhod2 signal. (*Inset*) Conversion of both signals to free Ca^{2+} and adjustment of GCaMP2 signal for association and dissociation kinetics.

delayed fluorescence transitions in GCaMP2 (Fig. 4 *a* and *b* and Table 2). Of interest was the absence of the prominent Ca^{2+} dependence of the association time constant of GCaMP1, which increases steeply below $\approx$400 nM (11); fluorescence on and off rates for GCaMP2 were equivalent over a 200-fold range of free Ca^{2+}. The more rapid and simpler kinetics of GCaMP2 at 37°C constitute a marked advantage for the measurement of rapid Ca^{2+} signals although, in the context of the rapidly beating mouse heart, fluorescence transitions in the ms range would be expected to produce predictable distortions of the underlying Ca^{2+} transients at higher rates.

To determine the effect of slower fluorescence transitions of GCaMP2 on rapid heart Ca^{2+} transients, we measured Ca^{2+} signals in paced hearts from ccGC2 mice transiently loaded with Rhod2, a fast Ca^{2+} indicator. GCaMP2 and Rhod2 fluorescent signals simultaneously recorded from the same array subregions provided a direct comparison of the raw signals. The dynamic range ($\Delta F/F_o$) of GCaMP2 was almost three times greater than observed for Rhod2 during cardiac cycles (data not shown); however, GCaMP2 fluorescence signals displayed a consistent, rate-dependent delay relative to the fast dye (Fig. 4*c*). In a series of experiments in hearts paced at 200-ms cycle length, the rise of the GCaMP2 raw fluorescent signal was 45% slower than the Rhod2 signal (38.2 $\pm$ 4.2 vs. 26.3 $\pm$ 2.8 ms), and the diastolic decay similarly prolonged. The lagging GCaMP2 signals were well explained by the slower fluorescence transition kinetics, because the converted Ca^{2+} signals matched when corrected by using fluorescent association and dissociation rate constants obtained experimentally (Fig. 4*c Inset*; Rhod 2 transition kinetics were submillisecond and could not be measured by stop-flow). At cycle lengths lower than $\approx$200 ms, a rise in basal fluorescence was observed proportional to the stimulation rate, indicating that complete decay of fluorescence did not occur during diastole. Ca^{2+} sparks were not observed in single, voltage-clamped myocytes enzymatically prepared from the hearts of double transgenic mice, a limitation shared by other small molecule

Table 2. GCaMP2 fluorescence time constants

Sample	Concentration	Temp., °C	τ_{on}, ms	$+\Delta Ca^{2+}$, nM	τ_{off}, ms	$-\Delta Ca^{2+}$, nM	No.
Cytosol	4× dilution	37	14.29 ± 0.30	0.02→240	75.19 ± 0.68	91→0.02	1
Cytosol	32× dilution	37	13.85 ± 0.22	0.02→240	78.62 ± 0.57	12.3→0.02	2
Cytosol	32× dilution	20	27.4 ± 1.28*	0.02→240	429 ± 1.47*	12.3→0.02	3
Purified	1 nM	37	15.50 ± 5.10	0.02→61	73 ± 0.767	2200→0.02	4

Average time constants were derived from stop-flow experiments with step changes of free Ca^{2+} as indicated. The last column refers to traces shown in Fig. 3, which are representative of each condition. Only temperature had a significant effect on fluorescence time constants (*, $P < 0.05$ by ANOVA).

Ca^{2+} indicators such as Fura2; bulk cytosolic transients were readily recorded in single myocytes (data not shown).

Conduction of Ca^{2+} Waves in the Embryonic Heart. Genetically encoded cell sensors are particularly useful in the dissection of the complex cellular interactions that occur during development. We examined GCaMP2 signals in spontaneously beating embryonic hearts by imaging open-chested embryos *in vivo* and *ex vivo*. Signals were augmented in embryos by mating mice homozygous for GCaMP2, with one parent also expressing tTA, resulting in embryos with two functional GCaMP2 alleles and markedly augmented transgene expression. Ca^{2+}-dependent fluorescent signals were robust across the surface of the tubular, unseptated heart beginning at embryonic day (e.d.) 10, shortly after regular contractions are initiated, a period in which only limited *ex vivo* optical measurements have been attempted (33, 34). We were particularly interested in understanding the mechanism of atrioventricular (AV) delay and the timing of development of a functional AV node. As shown in Fig. 5*a*, prominent Ca^{2+} waveforms initiated in the atria of spontaneously beating embryonic hearts were rapidly conducted across the atrial surface. A dramatic slowing of the conducted Ca^{2+} wave occurred in the region of the AV canal, which separates the common atrial and ventricular chambers (Fig. 5 *a* and *b* and Movie 3, which is published as supporting information on the PNAS web site). Ca^{2+} waves exiting from the AV canal region continued along the ventricular surface; rapid conduction occurred through the ventricle, indicating a functional connection of the AV conduction pathway to the His/Purkinje system, consistent with histological (35) and electrophysiological (33, 34) data. The rate of conduction through the AV canal was ≈10-fold slower than through the atrial and ventricular chambers, effectively delaying connection to the ventricular conduction pathway, because ventricular breakthrough occurred after transmission of the signal through the AV canal (Fig. 5*c*), providing a sufficient delay for effective mechanical pumping. At e.d. 10.5, the atria could be efficiently paced from the ventricles, and bidirectional conduction was observed through the AV canal (data not shown). A distinct surface pathway has been anatomically identified in the embryonic mouse heart and hypothesized to mediate AV conduction before formation of a functional AV node (35); and a similar region of slowed cardiac conduction has been documented in the chick heart (36) but has not previously been demonstrated in mammals. Cells in this tissue layer display a distinct genetic pattern (37) and are eliminated by programmed cell death by e.d. 13.5 in the mouse (35). Consistent with the timing of elimination of these cells, we observed a loss of surface conduction through the AV canal at e.d. 13.5 (Fig. 5*d*); surface conduction of the Ca^{2+} waves ends at a discrete ring and does not travel continuously along the ventricular wall (see also Movie 4, which is published as supporting information on the PNAS web site) but emerges at the apical ventricular surface after a slight distinct delay. Similarly, pacing of embryonic hearts from the ventricles did not result in retrograde conduction into the atria (data not shown), indicating development of effective unidirectional conduction. These data indicate the presence of an AV conduction pathway that connects to both ventricular myocardium and the developing conduction system, demonstrating the important functional role of AV canal conduction in the preseptated heart and lending functional support to the importance of AV canal developmental abnormalities in fetal and adult arrhythmias. Given

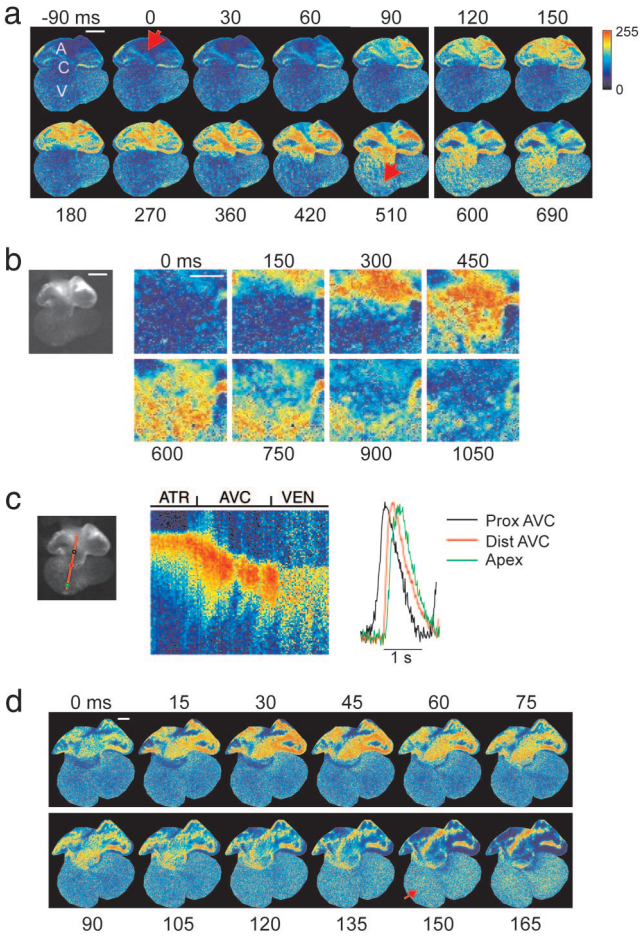

Fig. 5. Ca^{2+} Signaling in the developing heart. (a) Sequential images of activation of e.d. 10.5 heart during spontaneous beating (dorsal surface); A, atrium; C, canal; V, ventricle. Arrow in second image shows initial activation of atrium. Note slow passage of Ca^{2+} wave through the AV canal (AVC) and progression into ventricle. Ventricular activation at apex (arrow at 510 ms) occurs independently after passage through AVC. (*b*) Passage of cytosolic Ca^{2+} wave through the AVC region shown in box on image at *Left*. Shown is the e.d. 10.5 dorsal surface. (*c*) Virtual linescan (line of scan shown on image at *Left*; pseudolinescan in *Center*) taken from a 67-Hz series of images during spontaneous activation of an e.d. 10.5 heart. Ca^{2+} transients from the areas shown (circles) are shown at right. Note the short time interval between the beginning of the distal AVC and ventricular apex transients (ATR, atria; VEN, ventricle). (*d*) Images of Ca^{2+} fluorescence during spontaneous activation of an e.d. 13.5 heart (dorsal surface, 67 Hz). Note that Ca^{2+} wave ends in a ring at base of compacted AVC and does not extend into the ventricle. Arrow shows breakthrough of Ca^{2+} wave at ventricular apex. (Scale bars: 250 μm.) Color scale in *a* applies throughout.

PHYSIOLOGY

the difficulty in loading the heart without perfusion and the relatively slow spontaneous embryonic heart rate, ccGC2 mice will be particularly useful for the study of cardiac organogenesis.

Conclusions

We have demonstrated the use of a genetically encoded, high-signal Ca^{2+} indicator to monitor cellular Ca^{2+} signaling events *in vivo* and *in vitro* in the intact heart. The genetic Ca^{2+} sensor displays a relatively high signal over the physiological operating range of free $[Ca^{2+}]_i$ in the working heart, and interactions between endogenous proteins and the sensor domains of GCaMP2, which may underlie the marked discrepancy observed in the signal range of genetic indicators between transfected cells and transgenic mice (19, 20), do not seem to affect sensor function. The rapidly beating mouse heart represents perhaps the most challenging context for the use of an optical probe, because the requirement for high bandwidth measurements limits signal acquisition and the very short cardiac cycle length is on the order of magnitude of the fluorescent decay constant. Nonetheless, the reproducibility and high fidelity of signals obtained in ccGC2 mice at heart rates in excess of 300/min provide confidence that genetically encoded sensors will enable the measurement of Ca^{2+} and other cellular signals in virtually any mammalian organ system for which optical access can be obtained, providing a markedly expanded window of observations of physiological and pathophysiological cellular processes.

Materials and Methods

Generation of Tet-Off αMHC-CaMP2 Mice. The αMHC fragment containing seven tetO sequences (28) was ligated to a GCaMP2 BglII/NotI digestion product to αMHC-GCamP2. The 7,831-bp transgene was excised with NotI, gel purified, and injected into oocytes using standard techniques. Animals were genotyped by using primers for eGFP (18). Three lines were bred to tTA-αMHC mice to produce double transgenic mice. Transgene suppression was examined by addition of dox (1 mg/ml) in 2% sucrose in drinking water. Immunocytochemical methods were as described (38).

Ca^{2+}-GCaMP2-Binding Kinetics. Fluorescence association and dissociation was monitored in a stop-flow spectrofluorometer (Applied PhotoPhysics, Surrey, UK). Mouse hearts (2 ml volume) were suspended in 8 ml of buffer (200 mM sucrose/20 mM histidine, pH 7.2), homogenized with a Teflon glass homogenizer, and centrifuged at 2,000 × *g* for 20 min. Aliquots of Ca-EGTA-buffered solutions were added to the supernatant to clamp free Ca^{2+} at the desired level (39).

Optical Mapping. Hearts were perfused and suspended in a custom-designed optical chamber (32). Di-4-ANNEPS and Rhod2 loading, photodiode array mapping, restitution protocols, and analysis were as described (40). GCaMP2 was excited at 488 nm, and di-4-ANEPPS and Rhod-2 were excited at 530 nm. Emission was collected at >520 nm for eGFP, >610 nm for di-4-ANEPPS, and 585 nm for Rhod-2. Activation maps that included both the atria and ventricles (100 × 100 pixels) were captured with a CMOS camera (Micam Ultima; SciMedia, Irvine, CA) at ≥1 kHz. *In vivo* images were obtained by using a cooled charge-coupled device (CCD) camera (iXon; Andor Technology, South Windsor, CT) and acquired at 66 or 128 frames per s.

***In Vivo* Imaging.** Mice were time-mated, and embryos removed at the designated period of development by dissection from the uterus. Embryos were kept on ice until studied at 37°C in Tyrode's solution (136 mM NaCl/5.4 mM KCl/1 mM $MgCl_2$/0.33 mM NaH_2PO_4/2.5 mM $CaCl_2$/10 mM Hepes/10 mM glucose, pH 7.4) and imaged using a dissecting microscope (MSFLIII; Leica Microsystems, Heerbrug, Switzerland) and intensified charge-coupled device camera (iXon 860-BI; Andor Technology). Data were analyzed and processed by using customized MATLAB, IMAGEJ, or IDL routines. Color-coded images were normalized on a pixel-by-pixel basis throughout the series, setting the highest value to the maximum value, the lowest value to 0, and linearly scaling other values. Neonatal and adult mice were anesthetized with isofluorane and cannulated via tracheotomy. Positive pressure ventilation was initiated, and the chest was opened to expose the heart. Animals were maintained at 37°C with a heating pad, and ventilation frequency and tidal volume were adjusted to eliminate spontaneous breathing. The ventilator was briefly halted during image capture.

We thank Warren Zipfel, Mark Rishniw, and Geoffrey Eddlestone for helpful advice and Pat Fisher for immunocytochemistry. This work was supported by National Institutes of Health Grants HL45239, DK65992, and DK58795 (to M.I.K.) and HL69097, HL70722, and HL057929 (to G.S.), and a grant-in-aid from the Ministry of Education, Culture, Sports, Science, and Technology of Japan (to J.N.).

1. Berridge, M. J. & Irvine, R. F. (1984) *Nature* **312,** 315–321.
2. Tsien, R. W. & Tsien, R. Y. (1990) *Annu. Rev. Cell Biol.* **6,** 715–760.
3. Bootman, M. D. & Berridge, M. J. (1995) *Cell* **83,** 675–678.
4. Clapham, D. E. (1995) *Cell* **80,** 259–268.
5. Berridge, M. J., Bootman, M. D. & Lipp, P. (1998) *Nature* **395,** 645–648.
6. Grynkiewicz, G., Poenie, M. & Tsien, R. Y. (1985) *J. Biol. Chem.* **260,** 3440–3450.
7. Zhang, J., Campbell, R. E., Ting, A. Y. & Tsien, R. Y. (2002) *Nat. Rev. Mol. Cell Biol.* **3,** 906–918.
8. Miyawaki, A., Llopis, J., Heim, R., McCaffery, J. M., Adams, J. A., Ikura, M. & Tsien, R. Y. (1997) *Nature* **388,** 882–887.
9. Miyawaki, A., Griesbeck, O., Heim, R. & Tsien, R. Y. (1999) *Proc. Natl. Acad. Sci. USA* **96,** 2135–2140.
10. Baird, G. S., Zacharias, D. A. & Tsien, R. Y. (1999) *Proc. Natl. Acad. Sci. USA* **96,** 11241–11246.
11. Nakai, J., Ohkura, M. & Imoto, K. (2001) *Nat. Biotechnol.* **19,** 137–141.
12. Nagai, T., Sawano, A., Park, E. S. & Miyawaki, A. (2001) *Proc. Natl. Acad. Sci. USA* **98,** 3197–3202.
13. Heim, N. & Griesbeck, O. (2004) *J. Biol. Chem.* **279,** 14280–14286.
14. Kerr, R., Lev-Ram, V., Baird, G., Vincent, P., Tsien, R. Y. & Schafer, W. R. (2000) *Neuron* **26,** 583–594.
15. Higashijima, S. I., Masino, M. A., Mandel, G. & Fetcho, J. R. (2003) *J. Neurophysiol.* **90,** 3986–3997.
16. Fiala, A. & Spall, T. (March 18, 2003) *Sci. STKE.*, 10.1126/stke.2003.174.pl6.
17. Wang, J. W., Wong, A. M., Flores, J., Vosshall, L. B. & Axel, R. (2003) *Cell* **112,** 271–282.
18. Ji, G., Feldman, M., Deng, K. Y., Greene, K. S., Wilson, J., Lee, J., Johnston, R., Rishniw, M., Tallini, Y., Zhang, J., *et al.* (2004) *J. Biol. Chem.* **279,** 21461–21468.
19. Hasan, M. T., Friedrich, R. W., Euler, T., Larkum, M. E., Giese, G., Both, M., Duebel, J., Waters, J., Bujard, H., Griesbeck, O., *et al.* (2004) *PLoS. Biol.* **2,** 763–775.
20. Nagai, T., Yamada, S., Tominaga, T., Ichikawa, M. & Miyawaki, A. (2004) *Proc. Natl. Acad. Sci. USA* **101,** 10554–10559.
21. Pologruto, T. A., Yasuda, R. & Svoboda, K. (2004) *J. Neurosci.* **24,** 9572–9579.
22. Griesbeck, O., Baird, G. S., Campbell, R. E., Zacharias, D. A. & Tsien, R. Y. (2001) *J. Biol. Chem.* **276,** 29188–29194.
23. Reiff, D. F., Ihring, A., Guerrero, G., Isacoff, E. Y., Joesch, M., Nakai, J. & Borst, A. (2005) *J. Neurosci.* **25,** 4766–4778.
24. Siemering, K. R., Golbik, R., Sever, R. & Haseloff, J. (1996) *Curr. Biol.* **6,** 1653–1663.
25. Zacharias, D. A., Violin, J. D., Newton, A. C. & Tsien, R. Y. (2002) *Science* **296,** 913–916.
26. Ohkura, M., Matsuzaki, M., Kasai, H., Imoto, K. & Nakai, J. (2005) *Anal. Chem.* **77,** 5861–5869.
27. Diez-Garcia, J., Matsushita, S., Mutoh, H., Nakai, J., Ohkura, M., Yokoyama, J., Dimitrov, D. & Knopfel, T. (2005) *Eur. J. Neurosci.* **22,** 627–635.
28. Sanbe, A., Gulick, J., Hanks, M. C., Liang, Q., Osinska, H. & Robbins, J. (2003) *Circ. Res.* **92,** 609–616.
29. Waldo, K. L., Kumiski, D. H., Wallis, K. T., Stadt, H. A., Hutson, M. R., Platt, D. H. & Kirby, M. L. (2001) *Development (Cambridge, U.K.)* **128,** 3179–3188.
30. Colomer, J. M., Terasawa, M. & Means, A. R. (2004) *Endocrinology* **145,** 1356–1366.
31. Loew, L. M., Cohen, L. B., Dix, J., Fluhler, E. N., Montana, V., Salama, G. & Jian-young, W. (1992) *J. Membr. Biol.* **130,** 1–10.
32. Baker, L. C., London, B., Choi, B. R., Koren, G. & Salama, G. (2000) *Circ. Res.* **86,** 396–407.
33. Rentschler, S., Vaidya, D. M., Tamaddon, H., Degenhardt, K., Sassoon, D., Morley, G. E., Jalife, J. & Fishman, G. I. (2001) *Development (Cambridge, U.K.)* **128,** 1785–1792.
34. Rothenberg, F., Nikolski, V. P., Watanabe, M. & Efimov, I. R. (2005) *Am. J. Physiol Heart Circ. Physiol.* **288,** H344–H351.
35. Viragh, S. & Challice, C. E. (1977) *Dev. Biol.* **56,** 382–396.
36. de Jong, F., Opthof, T., Wilde, A. A., Janse, M. J., Charles, R., Lamers, W. H. & Moorman, A. F. (1992) *Circ. Res.* **71,** 240–250.
37. Franco, D., Lamers, W. H. & Moorman, A. F. (1998) *Cardiovasc. Res.* **38,** 25–53.
38. Xin, H. B., Deng, K. Y., Rishniw, M., Ji, G. & Kotlikoff, M. I. (2002) *Physiol. Genomics* **10,** 211–215.
39. Bers, D. M., Patton, C. W. & Nuccitelli, R. (1994) *Methods Cell Biol.* **40,** 3–29.
40. Baker, L. C., Wolk, R., Choi, B. R., Watkins, S., Plan, P., Shah, A. & Salama, G. (2004) *Am. J. Physiol Heart Circ. Physiol.* **287,** H1771–H1779.